Field-Tunable Interactions and Frustration in Underlayer-Mediated Artificial Spin Ice

Susan Kempinger,[1,2,*] Yu-Sheng Huang,[1] Paul Lammert,[1] Michael Vogel,[3] Axel Hoffmann,[4] Vincent H. Crespi,[1] Peter Schiffer,[5] and Nitin Samarth[1,†]

[1]*Department of Physics, The Pennsylvania State University, University Park, Pennsylvania 16802-6300, USA*
[2]*Department of Physics, North Central College, Naperville, Illinois 60540, USA*
[3]*Institute of Physics and Center for Interdisciplinary Nanostructure Science and Technology (CINSaT), University of Kassel, Heinrich-Platt-Straße 40, 34132 Kassel, Germany*
[4]*Materials Research Laboratory and Department of Materials Science and Engineering, University of Illinois at Urbana-Champaign, Urbana, Illinois 61801, USA*
[5]*Department of Applied Physics and Department of Physics, Yale University, New Haven, Connecticut 06520, USA*

(Received 3 April 2021; revised 24 July 2021; accepted 11 August 2021; published 10 September 2021)

Artificial spin ice systems have opened experimental windows into a range of model magnetic systems through the control of interactions among nanomagnet moments. This control has previously been enabled by altering the nanomagnet size and the geometry of their placement. Here we demonstrate that the interactions in artificial spin ice can be further controlled by including a soft ferromagnetic underlayer below the moments. Such a substrate also breaks the symmetry in the array when magnetized, introducing a directional component to the correlations. Using spatially resolved magneto-optical Kerr effect microscopy to image the demagnetized ground states, we show that the correlation of the demagnetized states depends on the direction of the underlayer magnetization. Further, the relative interaction strength of nearest and next-nearest neighbors varies significantly with the array geometry. We exploit this feature to induce frustration in an inherently unfrustrated square lattice geometry, demonstrating new possibilities for effective geometries in two-dimensional nanomagnetic systems.

DOI: 10.1103/PhysRevLett.127.117203

Custom-designed artificial magnetic materials provide model platforms for studying a variety of fundamental problems in magnetism and also form the basis for applications such as nonvolatile memory and spin-based logic. Examples include magnetic multilayers and heterostructures wherein interlayer and interfacial exchange coupling yields new magnetic behavior relevant to spintronic applications [1], continuous ferromagnetic films interfaced with patterned ferromagnetic arrays that allow systematic control over pinning of magnetic domain walls [2,3], and nanoscale ferromagnetic elements with mixed anisotropy that allow the engineering of spin frustration and spin texture [4]. Artificial spin ice (ASI) is another interesting example of a custom-designed magnetic material, in which interacting arrays of lithographically defined single domain nanomagnets are arranged in frustrated two-dimensional geometries [5–8]. A variety of fundamental phenomena have been studied in ASIs, including the physics of Dirac strings and magnetic monopoles [9–13], the interplay between frustration and thermal fluctuations [14,15], and unusual types of frustration [16,17]. Recent studies have investigated the ground states of ASI with broken rotational symmetry in arrays of in-plane nanomagnets [18,19]. ASI systems are also candidates for reconfigurable magnonics and neuromorphic computing [6–8].

Perpendicular anisotropy ASIs, in which the individual islands have perpendicular magnetic anisotropy (PMA) with moments pointing normal to the plane of the structure [20–22], are of particular interest since switching dynamics of the entire microstate can be probed in full detail using spatially resolved magneto-optical Kerr effect (MOKE) microscopy [23,24]. This is because the polar MOKE effect has a large enough magnitude to readily allow extreme diffraction-limited microscopy with the spatial resolution (~300 nm) required to measure the magnetic state of each individual island in an array as a continuous function of externally applied magnetic field. In this Letter, we show how the effective geometry of PMA artificial spin ice can be manipulated without changing the physical geometry by altering the interactions between islands.

We fabricated a composite system comprised of an array of ferromagnetic islands with PMA supported on a 15 nm continuous film of the soft ferromagnet $Ni_{0.80}Fe_{0.20}$, also known as permalloy (Py). In bit-patterned media and other hybrid systems, such underlayers have been shown to increase the interaction strength of arrays due to a magnetic mirroring effect [25–28]. Micromagnetic modeling has been used to show that for an in-plane artificial spin ice array, coupling to a soft underlayer leads to a complex system exhibiting dynamically coupled modes [29]. Because the underlayers must be soft enough to be affected

by the stray field of the magnetic islands, they can be biased by even a modest in-plane field. This breaks the lateral symmetry of the system, resulting in new ground state properties, including the ability to select *in situ* a subset of the microstates that the array can achieve during demagnetization. The underlayer also tunes the relative coupling strength of the nearest neighbors (NN) and next nearest neighbors (NNNs). For arrays with a square geometry, this is equivalent to changing the J_2/J_1 ratio, where J_1 and J_2 are the NN and NNN coupling constants, respectively, in the square Ising model [30–34], and we show experimentally that this geometry can be tuned such that $J_2/J_1 > 1$. Previous studies have looked at changing the J_2/J_1 ratio in in-plane artificial square ice [13,35], but the symmetry is much more complex in that case due to the in-plane moments. Our results demonstrate that soft ferromagnetic underlayers can be used to build highly tunable systems, both enabling model systems with properties that have not been experimentally realized otherwise and also opening the door to possible new applications.

We studied two separate samples of Pt/Co multilayer islands on Py underlayers, which were demagnetized and measured independently. We first deposited 15 nm thick Py underlayers using electron beam evaporation, and then we deposited and patterned Ti(2 nm)/Pt(10 nm)/$[\mathrm{Co}(0.3\ \mathrm{nm})/\mathrm{Pt}(1\ \mathrm{nm})]_8$ islands using electron beam lithography and dc sputtering. The islands were 425 nm in diameter, with lattice spacing ranging from 500 to 800 nm, in both frustrated (triangular) and unfrustrated (square) geometries. The triangular lattice had sixfold rotational symmetry, and the square lattice had fourfold rotational symmetry [see Fig. 1(a)]. We also studied kagome (frustrated) and hexagonal (unfrustrated) geometries, both of which are decimations of a triangular lattice. Data for these arrays are included in the Supplemental Material [36]. SEM imaging confirmed the size of the islands and showed that neighboring islands were well defined and separated [Fig. 1(b)].

To probe these systems, we used a custom-built diffraction-limited, polar MOKE microscope with a resolution of 300 nm to collect images of demagnetized states of arrays for different lattice types and spacings. The external field was controlled using a 2-pole projected field magnet (GMW5201) with a dominant perpendicular field component and a smaller in-plane component. We prepared the states with an oscillating, decreasing magnetic field protocol with a maximum applied field of 1.5 kOe and a step size of 2 Oe in the switching region, using in-plane field angles between −60° and 60°. Because the PMA structures are not robust against heating, this sort of demagnetization protocol is standard for preparing perpendicular anisotropy ASI in a low energy collective state [21].

In the extended arrays, we define θ to be the angle between the in-plane field component and one of the NN directions, as shown in Fig. 1. The coercive field of the

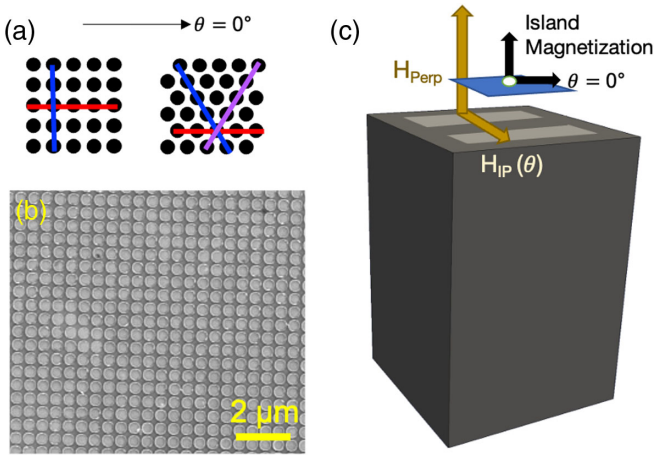

FIG. 1. (a) Square and triangular geometries with lines showing the NN directions. (b) Scanning electron microscope image of perpendicular magnetic anisotropy islands on Py in a square lattice array. (c) Schematic of sample over projected field magnet. The perpendicular (H_{Perp}) and in-plane (H_{IP}) components of the magnetic field are shown, along with the coordinate system relative to the sample (denoted by the island magnetization and $\theta = 0$ directions). The white dot represents the illuminated area for the MOKE studies.

array was around 800 Oe. The in-plane field is approximately 5% of the out-of-plane field and the coercivity and saturation field of the soft underlayer are very small (<10 and <25 Oe, respectively) and we do not expect them to vary significantly with θ. As a result, throughout the switching region, the in-plane field component is sufficient to saturate the soft underlayer and the magnetization direction of the underlayer is reversed with each reversal of the perpendicular field direction. The direction of the in-plane field component is controlled by rotating the magnet underneath the sample, as shown in Fig. 1(c). Large angular rotations of the magnet cause the sample to shift away from the pole and no longer experience a strong perpendicular field. To avoid potential influences of rotation on the Py reversal due to changes in the ratio of perpendicular and in-plane field strength, we restrict our measurements to rotation angles where the sample does not move away from the pole position of the magnet. Micromagnetic simulations demonstrated that the underlayer significantly enhances the interaction strength, as discussed in the Supplemental Material [36].

Figure 2 shows MOKE images of a triangular (a),(b) and a square (c),(d) array demagnetized at various in-plane field orientations. To generate images with strong magnetic contrast, we subtract images of the array in a saturated state from images in the demagnetized state. All images are taken in the remanent state. After the background subtraction, islands that are "up" and "down" appear light and dark, respectively. The Py magnetization is not visible, as it lies in the plane. In the triangular array, the variation in nearest neighbor correlation is observable by eye in images

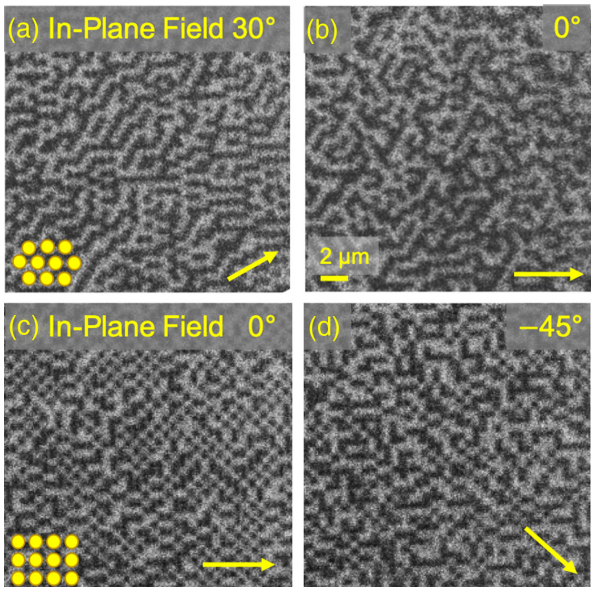

FIG. 2. MOKE images of perpendicular magnetic anisotropy artificial spin ice after demagnetization for triangular and square lattice geometries. Top row: Images of demagnetized 500 nm triangular array with in-plane field oriented at (a) $\theta = 30°$ and (b) $\theta = 0°$. Bottom row: MOKE images of demagnetized 500 nm square array with in-plane field oriented at (c) $\theta = 0°$ and (d) $\theta = -45°$. The dots in panel (a) and panel (c) represent the orientation of the lattices within the images.

of the different microstates. Figures 2(a) and 2(b) show the demagnetized state of a 500 nm spacing triangular array prepared with $\theta = 30°$ and 0°, respectively. We observe that the microstates at 30° have extended lines of aligned islands in the direction of the applied field. The microstate at −30° (not shown) is qualitatively similar. At $\theta = 0°$, however, the microstate appears more disordered. In the square array, the data with $\theta = 0°$ shows large patches of the ground state checkerboard pattern as expected. However, the −45° data appear quite different, with extended regions of aligned islands in the direction of the applied magnetic field, similar to the ordered state observed in the triangular array. It is visually apparent from the raw data that there is a significant impact on the microstate when the direction of the in-plane field is changed.

To characterize the order in these states, we calculate the NN correlation function

$$C_S = \langle S \rangle^2 - \sum_{i,j} S_i S_j. \tag{1}$$

The sum is taken over NN pairs, and S is the magnetization direction of each island (up or down, denoted as ± 1). This form matches the form used in previous publications [24]. $\langle S \rangle^2$ is nearly zero in demagnetized states and hence provides only a minor correction. The correlation values for samples with Py underlayers show a clear variation of C_S with in-plane field angle for all lattices considered [Figs. 3(a) and 3(c)]. The control samples without Py underlayers show no such variation [Figs. 3(b) and 3(d)]. The directional dependence is clearly an effect of the soft underlayer.

For the triangular array, the correlation is maximized at −30°, 30°, and 90°, i.e., when the field is normal to a NN direction. These correspond to the states with extended lines of aligned islands shown in Fig. 2(a). Similar behavior is seen in the other sixfold symmetric lattices discussed in the Supplemental Material [36]. At 0° and 60°, the field is oriented along a NN direction and normal to one of the *NNN* directions. These angles correspond to the disordered triangular state in Fig. 2(b). At these angles there is a decrease in NN correlation and a corresponding increase in next nearest neighbor (NNN) correlation. This variation becomes more pronounced at larger lattice spacings. This indicates that there might be a significant influence of NNN coupling on the demagnetized states of the array.

The correlation in the square array has a much larger θ dependence, which is accompanied by a dramatic variation in the NNN correlation. In the ground state, the NNN correlation is ferromagnetic, mediated by the antiferromagnetic NN correlation. However, when the field is aligned at ±45°, normal to an NNN direction, the NNN coupling becomes antiferromagnetic.

This rotational dependence of the correlation arises from the mutual influence of the magnetization in the underlayer and the magnetization in the islands. To model these effects, we turn to micromagnetic simulations. We used the micromagnetics package MuMax3 [37] to simulate a single pair of islands with and without a Py underlayer. Simulation data and details can be found in the Supplemental Material [36]. After demagnetization, the island-island interaction strength is greater with an underlayer due to the interaction between the Py and the islands. The magnetization in the islands is canted slightly in the direction of the underlayer magnetization, which causes an angle-dependent reduction from the maximum interaction strength. Simultaneously, the Py magnetization between islands cants away from saturation in plane toward alignment with the island's dipolar fields. The more aligned the underlayer magnetization is to the island dipolar field, the stronger the interactions are. To extrapolate from a single pair of islands to an extended line of islands, we used appropriate symmetry considerations along with an assumption that a demagnetized line of islands contains an approximately even mixture of up and down islands. These considerations are discussed in detail in the Supplemental Material [36]. Overall, there is a large peak in interaction energy when the in-plane component of the applied field is oriented perpendicular to the pair of islands, and a second, smaller peak in interaction energy when this field component is oriented parallel to the pair. This suggests that the moment correlation between islands

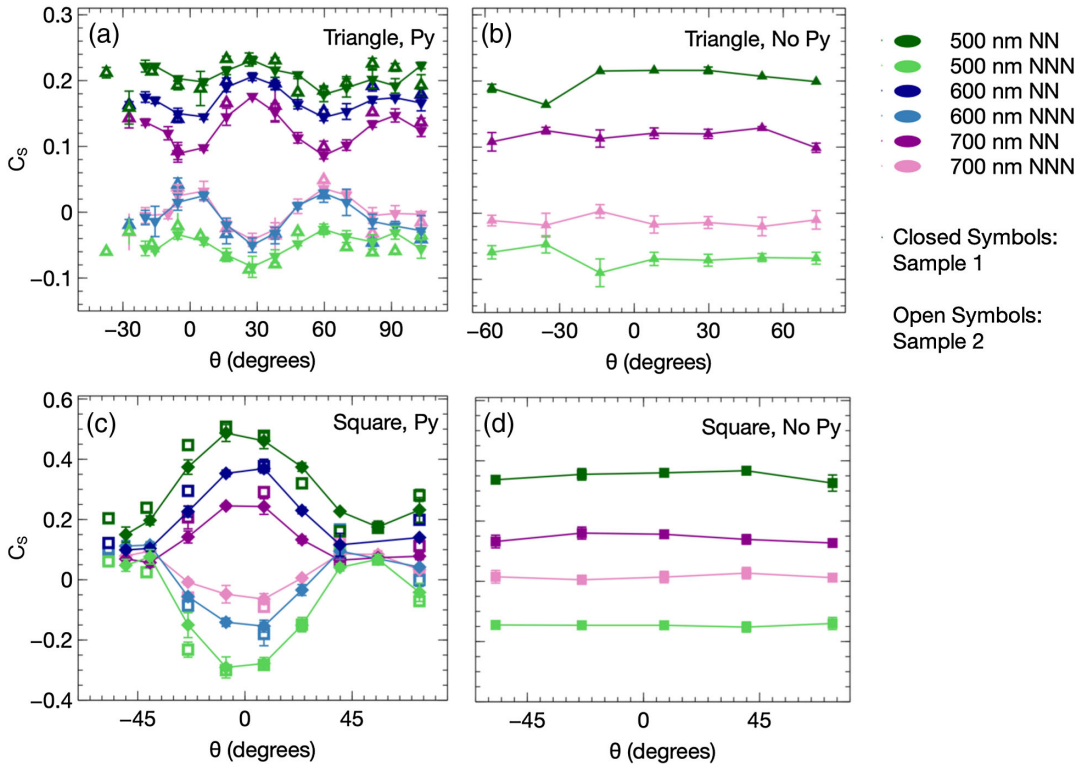

FIG. 3. Moment correlations of triangular and square arrays as a function of the direction of the in-plane component of the magnetic field during demagnetization, with and without permalloy underlayers.

which are nearest neighbors along an *arbitrary* direction D takes the form

$$C_{S,\text{directional}} = a\cos(2\phi) + b\cos(4\phi) + c, \qquad (2)$$

where ϕ is measured relative to the perpendicular to D.

Equation (2) gives us the information we need to additionally consider directional dependence of correlations. For the triangular lattice, we considered symmetry equivalent directions D1, D2, and D3 [Fig. 4(a), inset], aggregating the three datasets using the *relative* angles ϕ (rather than the absolute angle θ), and fit the aggregated data to Eq. (2) [see Fig. 4(b)]. Best fit parameters and χ^2 values can be found in Supplemental Material [36]. For the square lattice, directions D1 and D2 (Fig. 5) were treated similarly.

The directional correlation values for the triangular lattice match our visual observations of ordered states occurring at $\theta = -30°, 30°$. The average correlation (C_S) of a moment array with a frustrated geometry cannot exceed $1/3$, because the competing interactions prevent perfect ordering [21]. Without the soft underlayer, this average correlation is the same for all three NN directions (see Supplemental Material [36]). With the symmetry-breaking underlayer however, the maximum value of directional correlation ($C_{S,\text{directional}}$) in the triangular lattice reaches values as large as 0.55, as shown in Fig. 4(a). This increase of $C_{S,\text{directional}}$ in one direction leads to a suppression of $C_{S,\text{directional}}$ in other directions so that the average value of C_S obeys the appropriate limit. A high value of correlation occurs when there is strong antiferromagnetic ordering, which occurs in the direction perpendicular to the applied field, leading to the apparent chains of aligned islands in the applied field direction for angles with highly ordered states. Considering $C_{S,\text{directional}}$ as a function of interaction strength, we observe that the height of the main peak [0° in Fig. 4(b)] decreases steadily with decreasing interaction strength, while the minimum value consistently shows almost no correlation and the secondary peak [90° in Fig. 4(b)] maintains approximately the same height. The kagome lattice data show similar behavior (see Supplemental Material [36]). In contrast, the square array [Fig. 5(b)] and hexagonal array (see Supplemental Material [36]) show large, decreasing peaks, but also show an overall decrease in the minimum correlation and a suppression of the secondary peak with decreasing interaction strength.

The square lattice differs from all the other lattices considered in having fourfold, rather than sixfold, rotational symmetry. This is analogous to the square Ising model, with J_1 and J_2 representing NN and NNN coupling strength, respectively [30–34]. As shown in Fig. 3, both the NN and NNN correlations in this array show a pronounced variation with applied field angle. The variation in NNN correlation is strong enough to show a noticeable splitting between different NNN directions [N1 and N2, Fig. 5(c)]. For the 500 nm lattice spacing shown in the images in

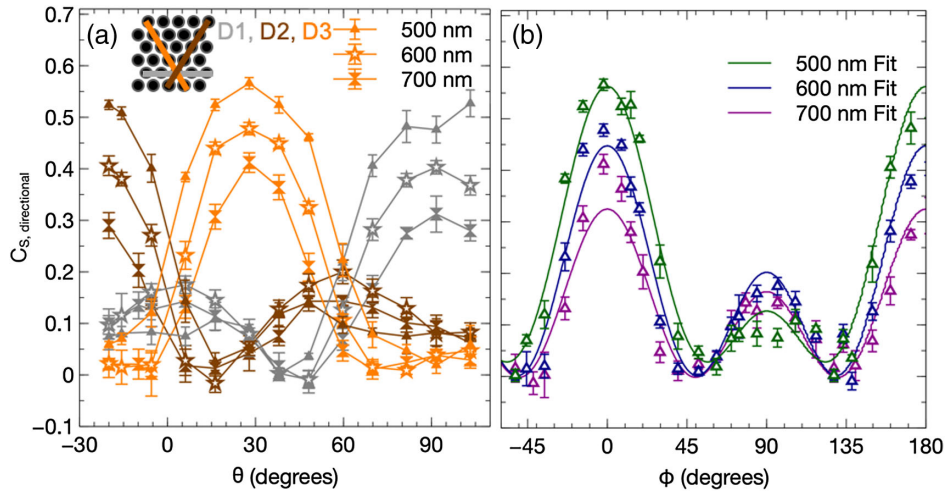

FIG. 4. (a) Correlation between nearest neighbors along the NN directions D1, D2, and D3 of the triangular lattice as a function of absolute field orientation θ for three different lattice spacings. (b) The same data aggregated by use of the *relative* angle ϕ (see text), with fits to Eq. (2).

Fig. 2, the NN and NNN correlation are not significantly different at points of minimum nearest-neighbor correlation. As the lattice spacing increases, we begin to observe points where the next-nearest-neighbor correlation exceeds the nearest neighbor correlation at the minimum values of NN correlation. If we take the correlation to be reflective of the effective interaction strength, i.e., J_1 and J_2, this indicates the existence of a crossover point where the NN and NNN interactions are balanced. At the crossover point there is an induced frustration in the array, because the system no longer has a preference between NN and NNN correlations. This explains why the square array demagnetized with $\theta = 45°$ looks qualitatively similar to demagnetized states of the triangular array. At an angle of 45°, the NN and NNN correlations differ least in the 500 nm lattice. Since the NN correlations are no longer dominant, the pattern of the demagnetized array is no longer best characterized as regions of the ground state. Instead, the induced frustration allows it to develop the same characteristics as the frustrated triangular array. The angle of the extended lines of islands is the visual manifestation of the splitting in NNN correlation.

The convergence (or even inversion) of the NN and NNN correlation values has interesting implications. The correlation values arise from the competition between interaction strength and disorder in the array. Disorder in artificial spin ice with perpendicular anisotropy is primarily a single-island property [23], which should not have a directional dependence. Therefore, within a single fabricated sample, the character of the variation in correlation as the in-plane field is rotated should be governed primarily by the island-island interaction, or J_1 and J_2. Our micromagnetic simulations also support this conclusion. From this, we conclude that as the NN and NNN correlation values

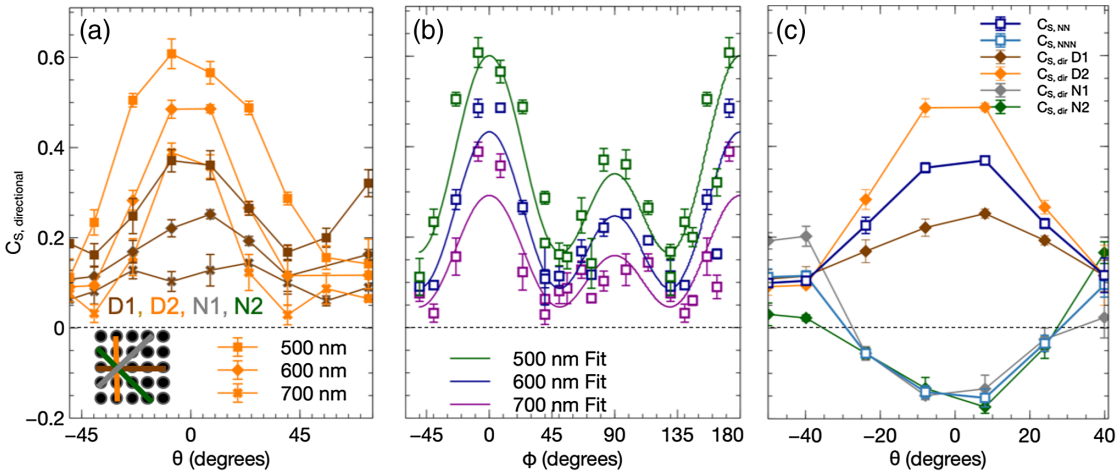

FIG. 5. (a) Correlation between nearest neighbors along the NN directions D1, D2 of the square lattice as a function of absolute field orientation θ for three different lattice spacings. (b) The same data aggregated by use of the *relative* angle ϕ (see text), with fits to Eq. (2). (c) Directional correlations for D1, D2, N1, and N2 for the 600 nm square array, along with overall NN and NNN correlation.

approach one another, the effective NN and NNN interactions, as modified by the underlayer, produce a system in which the distinction between NN and NNN is blurred, and insofar as correlation is concerned, effectively lost. This is equivalent to increasing J_2/J_1 until $J_1 = J_2$. As the NN and NNN correlation values invert, the system enters a state where $J_2 > J_1$. Such states have been studied in theory [38] and our material platform provides an experimental realization for studying these states.

Our results demonstrate that the addition of a soft magnetic underlayer to a perpendicular anisotropy ASI system enhances the interaction strength and breaks the rotational symmetry of the array by adding a directional dependence to the NN coupling and enhancing the NNN coupling. These two effects together cause the correlation in the array to vary with the angle of an in-plane field applied during demagnetization, providing a new mechanism through which to control the behavior of ASI systems, specifically the selection of a subset of available microstates during a demagnetization process. Both frustrated and unfrustrated lattices demonstrate a directional dependence of the correlation influenced by NNN correlations, and the frustrated lattices (triangular and kagome) show an increased impact of NNN effects as the lattice spacing is increased. The observation of a $J_2 > J_1$ state in a two-dimensional system indicates that this additional control will open the already-flexible ASI systems into a new dimension of parameter space that will allow the testing of spin models that would not otherwise be experimentally accessible. Furthermore, in this type of hybrid system the ASI nanoislands could potentially steer magnons in the underlayer, and the reconfigurable components of ASI with this additional degree of control could enhance the new device concepts that are being considered in neuromorphic computing and magnonics.

Sample design and MOKE measurement by S. K., Y. S. H., P. S., and N. S. was funded by the U.S. Department of Energy, Office of Basic Energy Sciences, Materials Sciences and Engineering Division under Grant No. DE-SC0010778 and subsequently DE-0020162. Sample fabrication by M. V. and A. H. at Argonne National Laboratory was supported by the U.S. Department of Energy, Office of Science, Basic Energy Science, Materials Science and Engineering Division. The use of the Center for Nanoscale Materials was supported by the U.S. Department of Energy (DOE), Office of Science, Basic Energy Science (BES), under Contract No. DE-AC02-06CH11357. We acknowledge DMR-1420620 for support of analysis and modeling efforts by P. L. and V. H. C.

*Corresponding author.
sekempinger@noctrl.edu
†Corresponding author.
nsamarth@psu.edu

[1] F. Hellman *et al.*, Interface-induced phenomena in magnetism, Rev. Mod. Phys. **89**, 025006 (2017).
[2] P. J. Metaxas, P.-J. Zermatten, J.-P. Jamet, J. Ferré, G. Gaudin, B. Rodmacq, A. Schuhl, and R. L. Stamps, Periodic magnetic domain wall pinning in an ultrathin film with perpendicular anisotropy generated by the stray magnetic field of a ferromagnetic nanodot array, Appl. Phys. Lett. **94**, 132504 (2009).
[3] A. Fraile Rodrguez, L. J. Heyderman, F. Nolting, A. Hoffmann, J. E. Pearson, L. M. Doeswijk, M. A. F. van den Boogaart, and J. Brugger, Permalloy thin films exchange coupled to arrays of cobalt islands, Appl. Phys. Lett. **89**, 142508 (2006).
[4] Z. Luo, T. P. Dao, A. Hrabec, J. Vijayakumar, A. Kleibert, M. Baumgartner, E. Kirk, J. Cui, T. Savchenko, G. Krishnaswamy, L. J. Heyderman, and P. Gambardella, Chirally coupled nanomagnets, Science **363**, 1435 (2019).
[5] R. F. Wang, C. Nisoli, R. S. Freitas, J. Li, W. McConville, B. J. Cooley, M. S. Lund, N. Samarth, C. Leighton, V. H. Crespi, and P. Schiffer, Artificial 'spin ice' in a geometrically frustrated lattice of nanoscale ferromagnetic islands, Nature (London) **439**, 303 (2006).
[6] S. H. Skjærvø, C. H. Marrows, R. L. Stamps, and L. J. Heyderman, Advances in artificial spin ice, Nat. Rev. Phys. **2**, 13 (2020).
[7] P. Schiffer and C. Nisoli, Artificial spin ice: Paths forward, Appl. Phys. Lett. **118**, 110501 (2021).
[8] L. J. Heyderman and R. L. Stamps, Artificial ferroic systems: Novel functionality from structure, interactions and dynamics, J. Phys. Condens. Matter **25**, 363201 (2013).
[9] S. Ladak, D. E. Read, W. R. Branford, and L. F. Cohen, Direct observation and control of magnetic monopole defects in an artificial spin-ice material, New J. Phys. **13**, 063032 (2011).
[10] E. Mengotti, L. J. Heyderman, A. F. Rodríguez, F. Nolting, R. V. Hügli, and H.-B. Braun, Real-space observation of emergent magnetic monopoles and associated Dirac strings in artificial kagome spin ice, Nat. Phys. **7**, 68 (2011).
[11] C. Phatak, A. K. Petford-Long, O. Heinonen, M. Tanase, and M. De Graef, Nanoscale structure of the magnetic induction at monopole defects in artificial spin-ice lattices, Phys. Rev. B **83**, 174431 (2011).
[12] L. A. Mól, R. L. Silva, R. C. Silva, A. R. Pereira, W. A. Moura-Melo, and B. V. Costa, Magnetic monopole and string excitations in two-dimensional spin ice, J. Appl. Phys. **106**, 063913 (2009).
[13] Y. Perrin, B. Canals, and N. Rougemaille, Extensive degeneracy, Coulomb phase and magnetic monopoles in artificial square ice, Nature (London) **540**, 410 (2016).
[14] V. Kapaklis, U. B. Arnalds, A. Farhan, R. V. Chopdekar, A. Balan, A. Scholl, L. J. Heyderman, and B. Hjörvarsson, Thermal fluctuations in artificial spin ice, Nat. Nanotechnol. **9**, 514 (2014).
[15] A. Farhan, P. M. Derlet, A. Kleibert, A. Balan, R. V. Chopdekar, M. Wyss, L. Anghinolfi, F. Nolting, and L. J. Heyderman, Exploring hyper-cubic energy landscapes in thermally active finite artificial spin-ice systems, Nat. Phys. **9**, 375 (2013).
[16] J. Drisko, T. Marsh, and J. Cumings, Topological frustration of artificial spin ice, Nat. Commun. **8**, 14009 (2017).

[17] C. Nisoli, V. Kapaklis, and P. Schiffer, Deliberate exotic magnetism via frustration and topology, Nat. Phys. **13**, 200 (2017).

[18] N. Keswani, R. Singh, Y. Nakajima, T. Som, and P. Das, Accessing low-energy magnetic microstates in square artificial spin ice vertices of broken symmetry in static magnetic field, Phys. Rev. B **102**, 224436 (2020).

[19] V. M. Parakkat, G. M. Macauley, R. L. Stamps, and K. M. Krishnan, Configurable Artificial Spin Ice with Site-Specific Local Magnetic Fields, Phys. Rev. Lett. **126**, 017203 (2021).

[20] E. Mengotti, L. J. Heyderman, A. Bisig, A. Fraile Rodríguez, L. Le Guyader, F. Nolting, and H. B. Braun, Dipolar energy states in clusters of perpendicular magnetic nanoislands, J. Appl. Phys. **105**, 113113 (2009).

[21] S. Zhang, J. Li, I. Gilbert, J. Bartell, M. J. Erickson, Y. Pan, P. E. Lammert, C. Nisoli, K. K. Kohli, R. Misra, V. H. Crespi, N. Samarth, C. Leighton, and P. Schiffer, Perpendicular Magnetization and Generic Realization of the Ising Model in Artificial Spin Ice, Phys. Rev. Lett. **109**, 087201 (2012).

[22] I. A. Chioar, N. Rougemaille, A. Grimm, O. Fruchart, E. Wagner, M. Hehn, D. Lacour, F. Montaigne, and B. Canals, Nonuniversality of artificial frustrated spin systems, Phys. Rev. B **90**, 064411 (2014).

[23] R. D. Fraleigh, S. Kempinger, P. E. Lammert, S. Zhang, V. H. Crespi, P. Schiffer, and N. Samarth, Characterization of switching field distributions in Ising-like magnetic arrays, Phys. Rev. B **95**, 144416 (2017).

[24] S. Kempinger, R. D. Fraleigh, P. E. Lammert, S. Zhang, V. H. Crespi, P. Schiffer, and N. Samarth, Imaging the stochastic microstructure and dynamic development of correlations in perpendicular artificial spin ice, Phys. Rev. Research **2**, 012001(R) (2020).

[25] D. Litvinov, R. M. Chomko, L. Abelmann, K. Ramstöck, G. Chen, and S. Khizroev, Micromagnetics of a soft underlayer, IEEE Trans. Magn. **36**, 2483 (2000).

[26] D. Litvinov, M. H. Kryder, and S. Khizroev, Recording physics of perpendicular media: Soft underlayers, J. Magn. Magn. Mater. **232**, 84 (2001).

[27] J. V. Ek, A. Shukh, E. Murdock, G. Parker, and S. Batra, Micromagnetic perpendicular recording model: Soft magnetic underlayer and skew effect, J. Magn. Magn. Mater. **235**, 408 (2001).

[28] M. T. Bryan, G. Heldt, T. Thomson, L. J. Heyderman, and G. Hrkac, Complex spin configurations in hybrid magnetic multilayer structures due to mutual spin imprinting, Phys. Rev. B **94**, 104415 (2016).

[29] E. Iacocca, S. Gliga, and O. G. Heinonen, Tailoring Spin-Wave Channels in a Reconfigurable Artificial Spin Ice, Phys. Rev. Applied **13**, 044047 (2020).

[30] D. P. Landau, Phase transitions in the Ising square lattice with next-nearest-neighbor interactions, Phys. Rev. B **21**, 1285 (1980).

[31] J. L. Morán-López, F. Aguilera-Granja, and J. M. Sanchez, First-order phase transitions in the Ising square lattice with first- and second-neighbor interactions, Phys. Rev. B **48**, 3519 (1993).

[32] A. Kalz, A. Honecker, S. Fuchs, and T. Pruschke, Phase diagram of the Ising square lattice with competing interactions, Eur. Phys. J. B **65**, 533 (2008).

[33] A. Kalz and A. Honecker, Location of the Potts-critical end point in the frustrated Ising model on the square lattice, Phys. Rev. B **86**, 134410 (2012).

[34] F. Kassan-Ogly, A. Murtazaev, A. Zhuravlev, M. Ramazanov, and A. Proshkin, Ising model on a square lattice with second-neighbor and third-neighbor interactions, J. Magn. Magn. Mater. **384**, 247 (2015).

[35] A. Farhan, M. Saccone, C. F. Petersen, S. Dhuey, R. V. Chopdekar, Y.-L. Huang, N. Kent, Z. Chen, M. J. Alava, T. Lippert, A. Scholl, and S. van Dijken, Emergent magnetic monopole dynamics in macroscopically degenerate artificial spin ice, Sci. Adv. **5**, eaav6380 (2019).

[36] See Supplemental Material at http://link.aps.org/supplemental/10.1103/PhysRevLett.127.117203 for additional simulated and experimental data.

[37] A. Vansteenkiste, J. Leliaert, M. Dvornik, M. Helsen, F. Garcia-Sanchez, and B. Van Waeyenberge, The design and verification of MuMax3, AIP Adv. **4**, 107133 (2014).

[38] A. Kalz, A. Honecker, and M. Moliner, Analysis of the phase transition for the Ising model on the frustrated square lattice, Phys. Rev. B **84**, 174407 (2011).